

# A Bidirectional Acid-Base Charging Model for Triboelectrification: part II. Experimental Verification by Inverse Gas Chromatography and Charging of Metal Oxides

Richard P. N. Veregin<sup>▲</sup>, Maria N. V. McDougall<sup>▲</sup>, Michael S. Hawkins, Cuong Vong and Vladislav Skorokhod  
Xerox Research Centre of Canada, Mississauga, Ontario L5K 2L1, Canada  
E-mail: rick.veregin@xrcc.xerox.com

Henry P. Schreiber

Department of Chemical Engineering, École Polytechnique, Université de Montréal, Montréal, Québec H3C 3A7, Canada

**Abstract.** Inverse gas chromatography (IGC) has been applied to study the surface properties of developer materials, measuring acid, base, and dispersion interactions. Model carrier and toner particles were prepared, where the toner was blended with various nanoparticulate metal oxide surface additives: Silica, titania, and alumina. Toner charging was determined with these surface additive formulations. IGC was used to characterize carrier and additive surface chemistry. Results from IGC were evaluated with respect to toner charge and to metal oxide work functions. A correlation was found between IGC-determined surface acid-base interaction parameters of the developer materials, and their work functions and triboelectric charge. Together, the IGC, work function, and charging results strongly support a work function model for developer charging, where the work function is determined by the acid and base properties of the developer components. Thus, as the ratio of the acid to base interaction parameters of the metal oxide surface additive increased, toner charge became more negative. The results are in quantitative agreement with the surface states charging model proposed in the companion paper in this series. © 2006 Society for Imaging Science and Technology.

[DOI: 10.2352/J.ImagingSci.Technol.(2006)50:3(288)]

## INTRODUCTION

Toner charging in two-component xerographic developers with metal oxide surface additives, such as SiO<sub>2</sub>, TiO<sub>2</sub>, and Al<sub>2</sub>O<sub>3</sub>, has been previously shown to be controlled by the oxide work function, as measured by Kelvin potentials.<sup>1</sup> The next question is: "What controls the oxide work function?" Indeed, the question has a broader scope, as it is not clear what controls the work function of any insulative material, if in fact, it even makes sense to ask the question about an insulator's work function. This question was potentially answered by a theoretical surface states model derived in a companion paper in this series.<sup>2</sup> Indeed, it was shown that surface parameters determined by IGC, in particular, the acid and base constants, represent the ability of any solid

insulative material to accept or donate electrons, respectively.<sup>3,4</sup> Thus, it was further shown that these constants can be related to both material work functions and to their ability to exchange charge on contact. In this paper, IGC has been used to study the surfaces of metal oxide additives and carrier in two-component xerographic developers. In addition, toner charge with the same metal oxide surface additives has been measured in two-component developers. Finally, the toner charge, as well as the previously determined oxide work functions, have been compared to the measured IGC surface acid base data, and to the predictions of the theoretical model.<sup>2</sup>

## EXPERIMENTAL

Contact potential differences (CPD) were measured previously at 20% and 80% RH, using a noncontact, electrostatic voltmeter.<sup>1</sup> The surface additives studied by CPD were Degussa A300™ SiO<sub>2</sub>, P25™ TiO<sub>2</sub>, and Al<sub>2</sub>O<sub>3</sub> C™. CPD values were extrapolated from 20% to 15% RH to enable comparison to charge and IGC data collected at 15% RH (a small correction). CPD values were converted to work functions using a CPD of +0.1 eV for the reference carbon black relative to Au,<sup>5</sup> and an Au work function of 4.46 eV (also measured by CPD<sup>6</sup>).

For triboelectric charge evaluation, all oxides were dry-blended on 4.6 μm poly(methylmethacrylate) PMMA model toner particles for 30 s at 15 krpm, with 100% toner surface coverage.<sup>7</sup> Also included in these charging studies were toners blended with Degussa R812™ and Wacker H2050™ silica. The carrier was a 65 μm irregular iron core powder-coated with 1 wt% of the same PMMA toner particles. The fused PMMA coating on the carrier surface covered more than 95% of the carrier core, as measured by scanning electron microscopy (SEM). Developers were prepared at 4% toner concentration (TC), equilibrated overnight at the desired RH, and then paint shaken for 15 min to reach equilibrium charge. Charge was measured by standard total blow-off tribo.<sup>8</sup>

<sup>▲</sup>IS&T Member

Received Mar. 21, 2005; accepted for publication Jul. 27, 2005.

1062-3701/2006/50(3)/288/6/\$20.00.

Acid and base interaction constants,  $K_a$  and  $K_b$ , respectively, and the surface is the dispersive surface energy of the solid,  $\gamma_s^d$ , were obtained from IGC measurements, following well established procedures.<sup>3,4,9,10</sup> The metal oxide and carrier stationary phases were packed in stainless steel columns, housed in a Varian 3400 gas chromatograph. Substrate temperatures ranged from room temperature to about 80 °C. RH was controlled by sweeping the columns with He carrier gas, which first passed through a dead space volume where RH was established with salt solutions of specific concentrations. The dispersive interaction capacity of the stationary phases was obtained from retention volumes of *n*-alkane probes, injected at extreme dilution. Polar vapors, selected from Gutmann's tabulations,<sup>3</sup> then led to evaluations of  $K_a$  and  $K_b$ . Retention volumes were collected in at least triplicate, with experimental uncertainties  $\leq \pm 4\%$ . The experimental uncertainty in acid-base parameters is about  $\pm 8\%$ .

## RESULTS AND DISCUSSION

### Inverse Gas Chromatography of Developer Materials

The accompanying paper<sup>2</sup> stated the basic equations from which may be obtained the surface characterization parameters:  $\gamma_s^d$ ,  $K_a$ , and  $K_b$ . In this approach, the solids are evaluated as stationary phases in the IGC experiment, measuring their interactions with various probe molecules, including nonpolar probes that can interact only via Lifschitz-van der Waals interactions, and polar probes that can also interact via acid-base interactions. An initial requirement is the generation of a linear relationship, at stated temperature,  $T$ , between a "descriptor" of the probes' chemistry and the measured retention volumes,  $V_n$ , of substrates for nonpolar (alkane) vapor probes. As noted in the accompanying paper, a thermodynamically justified descriptor is the cross-sectional area,  $a$ , of the vapor molecule in the adsorbed state. This choice poses practical problems, however. It is uncertain whether tabled values of  $a$ , valid for the molecule in their free-state, also apply when the vapor probe is adsorbed on a solid surface. Furthermore, a temperature dependence of  $a$  would need to be considered when IGC determinations span a significant  $T$  range. These difficulties may be overcome by using the normal boiling point,  $T_b$ , as the molecular descriptor of the vapors. A rationalization of this has been given by Panzer and Schreiber.<sup>10</sup> Accordingly, a linear plot is required when the retention volume  $\ln V_n$  is expressed as a function of  $T_b$ . An illustration is given in Fig. 1, the retention volumes of *n*-alkanes by a rutile ( $\text{TiO}_2$ ) stationary phase ( $RT \ln V_n$ ) are plotted against  $T_b$  of *n*-alkanes from C5 to C8 at 60 °C. The slope of the well-defined linear relationship then provides a measure of  $\gamma_s^d$ , the dispersion-force contribution to the surface energy of the solid. Also shown in the figure are the positions of  $V_n$  data for acidic and basic probes selected from the tabulation by Gutmann.<sup>3</sup> For simplicity, only two points are shown; they are for the acid benzene and the basic tetrahydrofuran, THF. Clearly, the rutile substrate interacts with both types of polar probe, since both the acid and the base generates  $V_n$  values greater than their nonpolar counterparts of equivalent  $T_b$ . Again

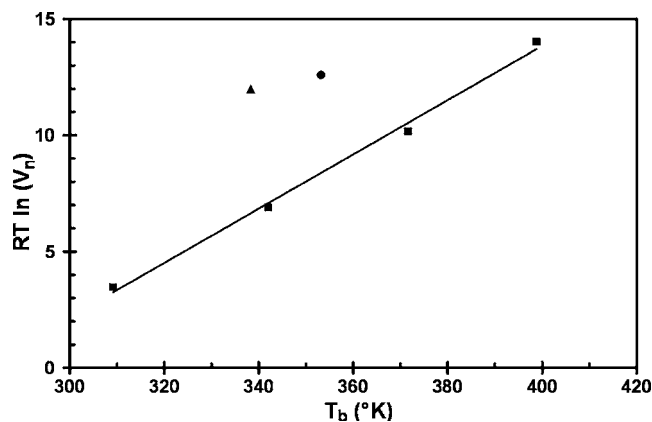


Figure 1. Logarithm of retention volume of probes on a rutile substrate plotted with the normal boiling point of the probe: ■ = *n*-alkanes, • = benzene, ▲ = THF.

following well-established protocols,<sup>4,9,10</sup> the normal distance of the polar probe positions from the reference line is the net free energy of desorption of the acid-base interactions,  $\Delta G^{ab}$ . This quantity is also measured at neighbor temperatures (55 °C and 65 °C in this instance), allowing for the construction of  $\Delta G^{ab}$  versus  $1/T$  for each of the polar probes, as mandated by the equations given in the preceding paper. The enthalpy datum ( $\Delta H^{ab}$ ) so determined is then used in conjunction with Gutmann's<sup>3</sup> AN and DN indexes for the vapor probes (respectively, 8.2 and 0.1 for benzene and 8.0 and 20 for THF) to obtain the acid/base parameters,  $K_a$  and  $K_b$  of the solid ( $\text{TiO}_2$ ). This uses representations of  $\Delta H_{ab}/AN$  versus  $DN/AN$ , as specified in the preceding article. The procedures described yield the following results for the rutile substrate, valid at the mean temperature of 60 °C:  $\gamma_s^d = 39.7 \text{ mJ/m}^2$ ;  $K_a = 2.3$ ;  $K_b = 2.8$ . Analogous approaches were employed to measure surface energy,  $K_a$  and  $K_b$  values for the materials of this work over the temperature range of interest.

### An Acid-Base Charge Model

The companion paper<sup>2</sup> showed in detail that we can fully describe an insulators' surface in terms of three parameters,  $\gamma_s^d$ ,  $K_a$ , and  $K_b$ , the surface interaction energy, and the acid constant and the base constants, where an acid is any electron acceptor and a base is any electron donor. Further since  $\gamma_s^d$  represents long-range Lifschitz-van der Waals forces, and thus does not involve electron donation and acceptance interactions, they do not exchange charge. Acid and base constants  $K_a$  and  $K_b$ , which represent short-ranges forces, and do involve electron donation and acceptance, must both be involved in charge exchange. Within the high density of states model, it was shown that the work functions of any material involved in the charging process, can be written in terms of the  $K_a$  and  $K_b$  values for those materials.<sup>2</sup> This is not possible in the low density of states model, as it is not possible to directly assign the measured IGC surface parameters with both work functions and density of states. However, *vide infra*, we will show that the analysis of IGC data is

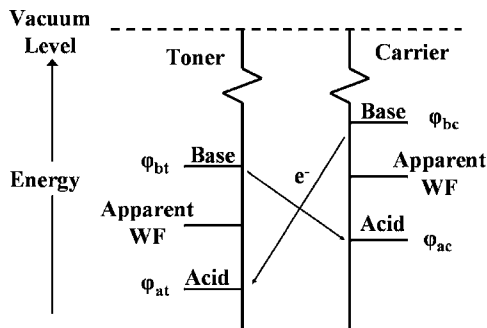


Figure 2. Toner-carrier charge exchange interactions. Arrows show the direction of the electron flow.

totally consistent with the high density surface-state charge model.

Briefly, the high density surface-state charge model<sup>11</sup> gives the toner charge shown in Eq. (1):

$$\text{Toner } q/m = A(\phi_c - \phi_t). \quad (1)$$

Equation (1) can be rewritten<sup>2</sup> in terms of the acid and base parameters, as in Eq. (2):

$$\text{Toner } q/m = - (A/2)kT[\ln(K_{at}/K_{bt}) - \ln(K_{ac}/K_{bc})]. \quad (2)$$

Here  $\phi_t$  and  $\phi_c$  are toner and carrier work functions,  $K_{at}$  and  $K_{bt}$  are the acid and base constants for the toner surface, and  $K_{ac}$  and  $K_{bc}$  are the acid and base constants for the carrier surface, respectively (Fig. 2). The factor  $A$  is a composite of a number of terms,<sup>2</sup> and is constant under the conditions of this study, which fixed toner/carrier geometry, as well as TC, at an equilibrium charge. Note that the work functions are defined here as positive numbers, so that a larger number represents lower energy. Thus, a more positive work function for toner compared to carrier gives a negative toner charge. The “effective” work function for a surface,  $\phi_s$ , is then the average over acid and base sites of that surface:

$$\phi_s = \phi^0 + \frac{1}{2}kT \ln(K_{as}/K_{bs}). \quad (3)$$

Here  $\phi^0$  is a constant, representing the work function of the reference state for the  $K_{as}$  and  $K_{bs}$  values, which can be obtained from the fit of Eq. (3) to the experimental data. The model is illustrated in Fig. 2.

As shown in the companion paper, this acid-base bidirectional charge model, as described by Eqs. (2) and (3), makes a number of predictions. The intent of the work herein is to test these predictions for a two-component xerographic developer, where the toner charge is controlled by the oxide surface additives.

#### Work Functions and Acid-Base Equilibria for Metal Oxide Particles

Work functions of hydrophilic oxides,  $\text{SiO}_2$ ,  $\text{TiO}_2$ , and  $\text{Al}_2\text{O}_3$ , were previously shown to correlate well with toner charge, where the oxides were toner surfaces additives.<sup>1</sup> This result was in agreement with the standard high-density of states model shown in Eq. (1). In the current work, the

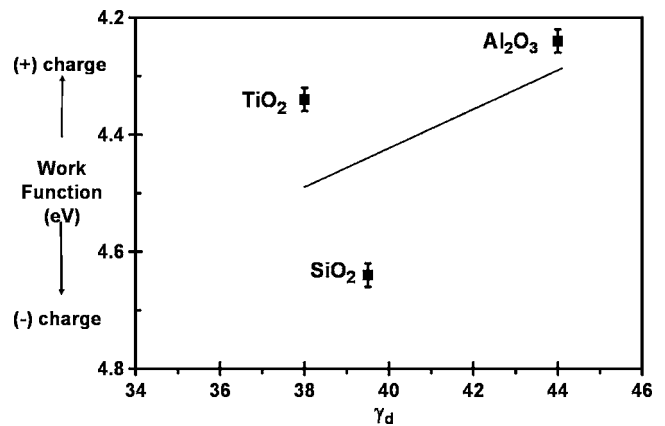


Figure 3. Work functions of untreated oxides plotted with oxide  $\gamma_d^s$  values.

intent is to extend this relationship of metal oxides and toner charge, to show that both the charge and the work functions are determined by the  $K_a$  and the  $K_b$  of the metal oxide particles and the carrier. To this end, the toner particles and the carrier coating were prepared from the same resin particles—both are PMMA. Thus, the toner charge is completely controlled by the surface metal oxide, as the base toner particle and carrier particle surfaces are identical, therefore,  $\phi_t = \phi_{\text{oxide}}$ . This was verified by confirming that base toner particle charge with the carrier was zero. The base toner particles in this study were then covered with the metal oxide surface additives, so that the only charge in the developer is that developed between the carrier and the metal oxide particles on the toner. Corresponding to the toner charging experiments, the oxide surface acid and base constants,  $K_a$  and  $K_b$ , and  $\gamma_d$  were determined by IGC measurements.

#### Effect of Oxide $\gamma_d$ on Work Functions

According to our model,<sup>2</sup>  $\gamma_d^s$  should not affect oxide work functions, as long-range Lifschitz-van der Waals forces do not involve charge exchange. The plot of work functions of the three metal oxides with  $\gamma_d^s$ , shown in Fig. 3, does not provide an apparent correlation, with  $r^2=0.250$ , as expected.

#### Effect of Oxide $K_a$ or $K_b$ on Work Functions

According to the model, neither of  $K_a$  or  $K_b$  alone should predict oxide work functions, provided, of course, that there is a sufficient range of both  $K_a$  and  $K_b$  for the oxides investigated. Figures 4 and 5 show, respectively, the plots of oxide work functions with  $K_a$  and  $K_b$ . In Fig. 4,  $K_a$  values for the oxides vary from 1.4 to 3, and in Fig. 5,  $K_b$  values vary from 1.8 to 3.1. These values do indeed cover a significant range of reported  $K_a$  and  $K_b$  values.<sup>4</sup> Although no comprehensive tabulation has been published, various authors have shown these parameters range from 0 to greater than 10 in highly polar materials such as cellulose and oxidized polymeric fibers. As expected with the proposed model, neither the  $K_a$  values in Fig. 4 nor  $K_b$  values in Fig. 5 alone can explain oxide work functions, both showing poor correlations, with  $r^2=0.48$  and  $r^2=0.59$ , respectively.

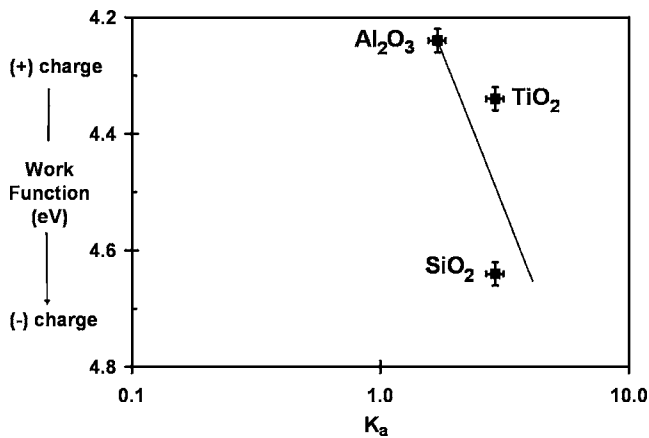


Figure 4. Work functions of untreated oxides plotted with the logarithm of oxide  $K_a$  values.

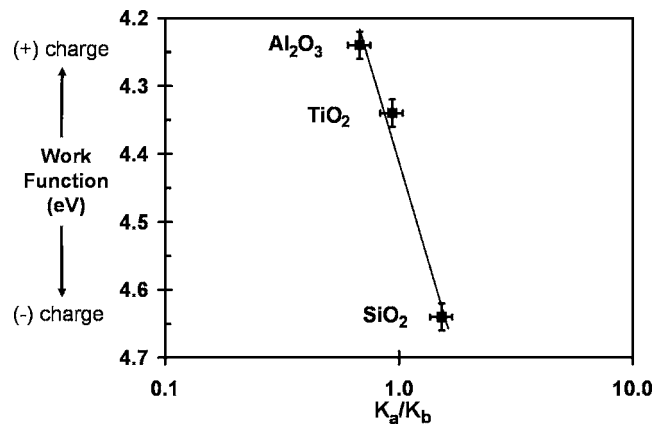


Figure 6. Work functions of untreated oxides plotted with the logarithm of oxide  $K_a/K_b$  values.

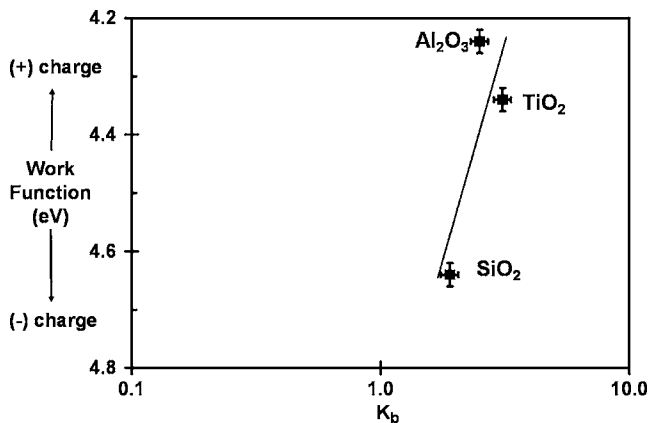


Figure 5. Work functions of untreated oxides plotted with the logarithm of oxide  $K_b$  values.

#### Effect of Oxide $K_a/K_b$ Ratio on Work Functions

The proposed model predicts that the oxide work functions should be dependant on the corresponding oxide  $K_a/K_b$  values. Figure 6 shows the plot of oxide work functions with the oxide  $K_a/K_b$  values. The plot shows an excellent linear correlation of oxide work function with the  $\ln(K_a/K_b)$  for the oxide, as predicted by Eq. (3), with an  $r^2=0.975$ , with all data fitting this relationship within the experimental error of the data. The fitted equation is:

$$\phi_s = 0.50 \ln(K_a/K_b) + 4.41. \quad (4)$$

Also, as expected from the proposed model, the larger the  $K_a/K_b$  ratio, the larger the work function. From the plot the measured  $\phi_s^0$ , as defined in Eq. (3), is 4.41: the work function value for  $\ln(K_a/K_b)=0$ .

Also, from the plot in Fig. 6, the slope is 0.5 eV. The predicted slope from Eq. (3) is  $kt/2=0.013$  eV. The reason for more than an order of magnitude difference in predicted and observed slope is not clear. However, it must be noted that  $K_a$  and  $K_b$  were determined by the interaction of surface states with gaseous probe molecules of cross-sectional area

$a$ , using the IGC method. We assume that these states that interact with the probe are the states that represent the measurable work functions, since we do see a strong correlation between the work functions and these acid-base interaction constants. However, the difference in slope we see here would suggest that the interaction of the molecular probe with the surface is less energetic than the work function of these surface states would indicate. There are a number of possible reasons for this. One possibility is that the acid-base interactions that are measured by IGC represent but a fractional electron transfer from the donor to the acceptor,<sup>3</sup> and thus presumably would not fully reflect the work functions of the donor and acceptor. That is, the measured work function is the energy required to emit a single electron to the vacuum level, so the interaction measured by IGC would represent the energy to transfer an average fractional electron charge of  $0.013/0.5=0.026$  in the acid-base interaction. A second possibility is that the work function datum is a much more sensitive probe of the surface than is the IGC datum. We really have a hierarchy of surface analyses: The droplet approach of contact angle measurements, for example, necessarily reports on a broad average of surface energetics. IGC does better, in that the much smaller molecular probe is capable of interacting more specifically with high energy sites of a surface. However, given the size of the IGC probe, it may be that IGC probes less deeply into the surface site energy distribution than the work function does, underestimating the energy of the interaction.

#### Toner Charging and Acid-Base Equilibria Metal Oxide Particles and Carrier Particles

Equation (2) predicts that toner charge with fixed carrier will be zero when  $\ln(K_{at}/K_{bt})=\ln(K_{ac}/K_{bc})$ . That is, net charge exchange will be zero when the toner and carrier acid/base ratios match. Equation (2) also predicts that negative toner charge will increase linearly with the oxide  $\ln(K_a/K_b)$  values from that zero charge point.

Figure 7 shows the plot of charge for toners with the untreated hydrophilic  $SiO_2$ ,  $TiO_2$ , and  $Al_2O_3$  surface additives, plotted against the oxides' respective  $K_a/K_b$  values. As

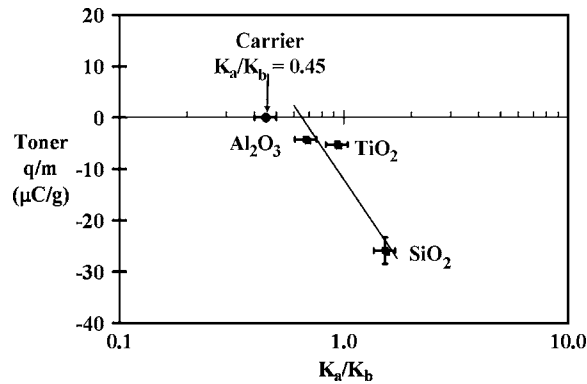


Figure 7. Toner charge with untreated oxide additives plotted with the logarithm of oxide  $K_a/K_b$ , as predicted by Eq. 6.

predicted, the negative toner charge with the oxide does increase linearly as the oxide  $\ln K_a/K_b$  ratio increases, with a good correlation coefficient of  $r^2=0.87$ . Also, the point of zero charge, as extrapolated from the oxide  $K_a/K_b$  values, is 0.69 (the 95% confidence limits are 0.57 and 0.82). As predicted by Eq. (2) the carrier  $K_a/K_b$  value of  $0.45 \pm 0.10$  matches the point of zero toner charge, within the 95% confidence levels. Thus, the toner charge is zero when the toner and carrier acid-base ratios are equal.

Since there appears to be a 1:1 relationship of the carrier  $K_a/K_b$  values and those of the metal oxide  $K_a/K_b$  values in charging (Fig. 7), and since the work functions of the metal oxides are related as well to the oxide  $K_a/K_b$  values (Fig. 6), this would indicate the  $K_a/K_b$  values for the carrier PMMA coating can be used to predict the work function of PMMA. Using the carrier values of  $K_a/K_b$  and Eq. (4), gives a PMMA work function of 4.0 eV. While measuring PMMA work functions directly is difficult, in contact charging with metals PMMA has been shown to donate electrons to metals of work function greater than 4 eV, but to accept electrons from metals of work function less than 4 eV,<sup>12</sup> in excellent agreement with the calculated work function from the  $K_a/K_b$  value.

While the data plotted in Fig. 7 is compelling, further work was done to extend the range of charge and  $K_a/K_b$  values, by studying the charging with two additional silica surface additives: Wacker H2050™  $\text{SiO}_2$  and Degussa R812™  $\text{SiO}_2$ . Unlike the three previous oxides studied, these oxides are not native untreated oxides, but rather are surface treated with silane coupling agents to render them more hydrophobic and to control their charging. The toner charge and the acid/base parameters were measured for these two additional oxides.

Toner  $q/m$  is plotted with  $\ln(K_a/K_b)$  for all five oxides, the original three hydrophilic oxides, and the two additional hydrophobic oxides, shown in the plot in Fig. 8. As predicted, the toner charge is linear with  $\ln(K_a/K_b)$ , with  $r^2=0.93$ . Also, the two additional data points follow closely that of the initial three hydrophilic oxides shown in Fig. 7. The best fit line in Figs. 7 and 8 are nearly identical. Again, negative toner charge increases with oxide acid-base ratio, as

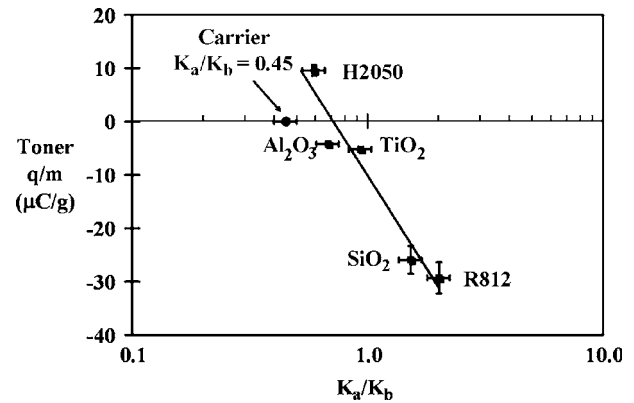


Figure 8. Toner charge with surface oxide additives plotted against  $\log(K_a/K_b)$ , including both untreated native oxides and treated hydrophobic oxide additives.

predicted. The point of zero toner charge shown in Fig. 7 is a  $K_a/K_b$  of 0.73 (95% confidence limits are 0.55 and 0.96), compared to the carrier  $K_a/K_b$  of  $0.45 \pm 0.10$ . Within 95% confidence levels, zero charge is observed at the predicted  $K_{at}/K_{bt}=K_{ac}/K_{bc}$ . Thus, again no electron transfer occurs if carrier and toner acid-base ratios match, while charge increases linearly with the difference in  $\log(K_a/K_b)$  between carrier and toner.

## CONCLUSIONS

Xerographic carrier and toner surface additives have been evaluated for surface acid/base properties using IGC, and for developer charging. The data are consistent with our previously developed model for charging of xerographic developer materials, which proposed bidirectional electron transfer from toner basic sites to carrier acidic sites, and from carrier basic sites to toner acidic sites. The result is an observed “effective” work function that is the average of the work functions of the acid and base sites of each material in the charge exchange. Thus, the observed work function and toner charge are determined by the relative amounts of these two electron exchange processes. As predicted by the model, the metal oxide measured work function increases with the logarithm of the ratio of surface acid to base constants for the oxide, as determined by IGC. Also, as predicted by the model, negative toner charge increases linearly with the logarithm of the ratio of the toner acid-base constants. The toner charge is zero when the toner and carrier acid-to-base ratios are identical. This also shows that the model also is consistent with the acid-base constants for the carrier coating as controlling factors for the carrier charging in the two-component developer. Thus, the acid-base constants are also predictive of the charging of polymer surfaces, as well as for metal oxide surfaces. Indeed, the acid-base constants enabled prediction of the PMMA work function, giving a result that is consistent with that derived based on contact charging with metals of varying work function. Finally, as the measured  $K_a$  and  $K_b$  values for the metal oxide additives, and PMMA coated carriers, represent donation and acceptance of electrons, the data herein thus supports an electron transfer mechanism for charging in these materials.

## REFERENCES

- <sup>1</sup>R. P. N. Veregin, D. Powell, C. P. Tripp, M. N. V. McDougall, and M. Mahon, *J. Imaging Sci. Technol.* **41**, 192 (1997).
- <sup>2</sup>R. P. N. Veregin, M. N. V. McDougall, M. Hawkins, C. Vong, V. Skorokhod, and H. P. Schreiber, *J. Imaging Sci. Technol.* **50**, 282 (2006).
- <sup>3</sup>V. Gutmann, *Donor-Acceptor Approach To Molecular Interactions* (Plenum Press, New York, 1978).
- <sup>4</sup>P. Mukhopadhyay and H. P. Schreiber, *Colloids Surf., A* **100**, 47 (1995).
- <sup>5</sup>P. C. Julien, *Carbon Black Science and Technology*, 2nd ed. (Marcel Dekker, New York, 1993), p. 410.
- <sup>6</sup>O. Klein and E. Lange, *Z. Elektrochem. Angew. Phys. Chem.* **44**, 542 (1938).
- <sup>7</sup>T. M. Jones and N. Pilpel, *J. Pharmacol.* **17**, 440 (1965).
- <sup>8</sup>L. B. Shein and J. Cranch, *J. Appl. Phys.* **46**, 5140 (1975).
- <sup>9</sup>C. Saint-Flour and E. Papirer, *J. Colloid Interface Sci.* **91**, 63 (1983).
- <sup>10</sup>U. Panzer and H. P. Schreiber, *Macromolecules* **25**, 3633 (1983).
- <sup>11</sup>E. J. Gutman and G. C. Hartmann, *J. Imaging Sci. Technol.* **36**, 335 (1992).
- <sup>12</sup>C. B. Duke and D. K. Davies, *J. Appl. Phys.* **49**, 315 (1978).